Journal of Magnetism and Magnetic Materials 343 (2013) 138–143

Contents lists available at SciVerse ScienceDirect

Journal of Magnetism and Magnetic Materials

journal homepage: www.elsevier.com/locate/jmmm

Synthesis and characterization of Fe_3O_4 nanoparticles coated with fucan polysaccharides

V.A.J. Silva [a,b], P.L. Andrade [a,b], M.P.C. Silva [b,c], A. Bustamante D. [d], Luis De Los Santos Valladares [b,e], J. Albino Aguiar [a,f,*]

[a] Programa de Pós-Graduação em Ciências de Materiais, Centro de Ciências Exatas e da Natureza, Universidade Federal de Pernambuco, 50670-901 Recife-PE, Brazil
[b] Laboratório de Imunopatologia Keizo Asami (LIKA), Universidade Federal de Pernambuco, 50670-901 Recife-PE, Brazil
[c] Departamento de Bioquímica, Universidade Federal de Pernambuco, 50670-420 Recife-PE, Brazil
[d] Laboratorio de Cerámicos y Nanomateriales, Facultad de Ciencias Físicas, Universidad Nacional Mayor de San Marcos, Ap. Postal 14-0149 Lima, Peru
[e] Cavendish Laboratory, University of Cambridge, J.J. Thomson Avenue, Cambridge CB3 0HE, United Kingdom
[f] Departamento de Física, Universidade Federal de Pernambuco, 50670-901 Recife-PE, Brazil

ARTICLE INFO

Article history:
Received 25 July 2012
Received in revised form
17 April 2013
Available online 29 April 2013

Keywords:
Magnetic nanoparticle
Magnetite
Fucan

ABSTRACT

In this work we report the preparation of fucan-coated magnetite (Fe_3O_4) nanoparticles by the co-precipitation method. These nanoparticles were characterized by scanning electron microscopy, transmission electron microscopy, X-ray diffraction (XRD), Fourier transform infrared (FT-IR) spectroscopy, Mössbauer spectroscopy and magnetic measurements. The nanoparticles showed quasi-spherical morphology with mean sizes around 10 nm. XRD and FT-IR confirmed the functionalization of the Fe_3O_4 nanoparticles with the fucan polysaccharide. Room temperature magnetization measurements and Mössbauer spectroscopy showed that the nanoparticles exhibited superparamagnetic behavior at 300 K and the magnetic properties of the Fe_3O_4 are partly screened by the coating preventing aggregation.

1. Introduction

Magnetic nanoparticles (MNPs) can be manipulated under the influence of an external magnetic field. They are usually composed of magnetic elements, such as iron, nickel, cobalt and their respective oxides [1]. In contrast to bulk magnetic materials whose magnetic properties are influenced by the thermal motion between magnetic domains, magnetic nanoparticles show single magnetic domains with all the spins aligned. There is no magnetization interference between domain walls in the MNPs as in the case of bulk materials [2,3]. Therefore, due to their size, MNPs exhibit different electrical, chemical, magnetic and optical properties than in bulk size [4].

Iron oxides, such as magnetite (Fe_3O_4), are commonly used for the synthesis of magnetic nanoparticles. They present stable magnetic response, are biodegradable and biocompatible, and present superparamagnetic effects on magnetic resonance imaging (MRI) [5,6]. Magnetite nanoparticles possess further interesting properties due to the presence of iron cations in two valence states, Fe^{2+} and Fe^{3+}, in the inverse spinel structure [7].

In the recent years, superparamagnetic nanoparticles have been widely used in biology and medicine for different purposes, such as protein and enzyme immobilization, bio-separation, immunoassays, hyperthermia, drug delivery, magnetically enhanced transfection, tissue engineering and MRI [8–12]. Typically, for biomedical purposes, MNPs are often surface-coated in order to improve their stability and biocompatibility, and to achieve hydrophilicity and conjugating capability [10,13]. Several coating materials have been used to modify the surface chemistry of the MNPs, including organic polymers (e.g. dextran, chitosan, polyethylene glycol), organic surfactants (e.g. sodium oleate and dodecylamine), inorganic metals (e.g. gold), inorganic oxides (e.g. silica and carbon) and bioactive molecules and structures (e.g. liposomes, peptides and ligands/receptors) [1,14,15].

Coating MNPs has many advantages. Having a magnetic core encapsulated in a protective and even biocompatible skin, they can be semiconducting, insulating, or metalic [16]. In the case of biocompatible capping, the particles can be well dispersed, the oxidation can be prevented and an appreciable amount of drug can be loaded to the shell. With polymeric coating of the MNPs, lots of functional groups from the polymer could be used for further functionalization and thus to increase potentiality [17]. Usually, the magnetic nanoparticles tend to aggregate due to their large surface-area/volume ratio and due to magnetic dipole–dipole attraction between particles. This property limits their applications and,

* Corresponding author at: Departamento de Física, Universidade Federal de Pernambuco, Av. Prof. Moraes Rego, 1235, 50670-901 Recife, Pernambuco, Brazil. Tel./fax: +55 8121268412.
E-mail address: albino@df.ufpe.br (J. Albino Aguiar).

0304-8853/$ - see front matter © 2013 Elsevier B.V. All rights reserved.
http://dx.doi.org/10.1016/j.jmmm.2013.04.062

therefore, dispersion of the magnetic nanoparticles is a crucial step in their production [18]. Polymer shells can prevent aggregation and the MNPs can be handled in aqueous dispersion [17].

Fucoidans are water soluble sulfated polysaccharides with high molecular weight. They are the main constituents of brown algae and can be found also in some marine invertebrates [19–22]. Fucoidans are highly branched sulfated polysaccharides, mainly based on l-fucose units which form homofucans or heterofucans. Homofucans contain substantial amount of l-fucose and sulfate groups [23]. On the other hand, heterofucans are composed primarily of a repeating chain of fucose and other sugars (e.g. glucose, mannose, galactose and uronic acid) [24]. In both homofucans and heterofucans, fucose is also attached to this backbone, forming branching points at several chain sites [21]. All these complex polysaccharides show a wide variety of biological activities, such as anti-adhesive [25], anti-coagulant [26,27], anti-complementary [28], anti-oxidant [29], anti-proliferative [30], anti-thrombotic [31], anti-platelet aggregation [32], anti-tumor [33] and anti-viral properties [22,23,34]. Thus, obtaining MNPs coated with polysaccharides is attractive for medical applications.

In this paper, we report the preparation and characterization of MNPs coated with fucan polysaccharides. The samples were prepared by the co-precipitation method and characterized by scanning electron microscopy (SEM), transmission electron microscopy (TEM), X-ray diffraction (XRD), Fourier transform infrared (FT-IR) spectroscopy, Mossbauer spectroscopy and magnetic measurements.

2. Methodology

2.1. Materials

The alga *Sargassum cymosum* was collected from the south coast of Recife, Pernambuco, Brazil. In this work, acetone ($(CH_3)_2CO$; Vetec Chemical), ferric cloride hexahydrate ($FeCl_3.6(H_2O)$; Merck), ferrous chloride tetrahydrate ($FeCl_2.4(H_2O)$; Merck), ammonium hydroxide (NH_4OH; Vetec Chemical) and oleic acid ($C_{18}H_{34}O_2$; Nuclear) were used for sample treatment and sintering. All other reagents were of analytical grade.

2.2. Extraction and partial purification of fucan from S. cymosum

The dried pulverized algae (100 g) were immersed in 300 mL of acetone and stirred for 12 h to remove pigments and lipids. This process was repeated twice. Then, it was decanted and the residue was dried at 45 °C under aeration to obtain a ketonic powder. A solution of 0.15 M NaCl (250 mL) was added to the ketonic powder and the pH was adjusted to 8.0 with NaOH. The proteolysis of this ketonic powder was carried out by papain enzyme (15 mg/g of ketonic powder) and the mixture was incubated at 45 °C overnight. The supernatant was collected by centrifugation at 10,000 g for 10 min and dried in a lyophilizer Multi-Tainer (FTS Systems, INC).

2.3. Determination of neutral sugars in fucan

The content of sugars was determined by using phenol sulfuric acid ($C_{20}H_{32}N_2O_6S$) and following the same procedure suggested by Dubois et al. (1956) [35]. The sugar concentration was determined in mg/mL by glucose standard curve and the absorbance was taken at 490 nm. The experiments were carried out in duplicate.

2.4. Preparation of the magnetite nanoparticles

Aqueous suspension of magnetic nanoparticles was prepared by co-precipitation of Fe(III) and Fe(II) in the presence of NH_4OH and oleic acid following standard procedure [36]. The molar ratio used of this suspension was 1.1 M:0.6 M for Fe^{3+} and Fe^{2+}, respectively. The nanoparticles were prepared as follows: 10 mL of ferrous chloride, 10 mL of ferric chloride and 500 μL of oleic acid were added to 100 mL of distilled water under stirring. Then NH_4OH solution was added by drops to the mixture to raise the pH to 11.0 while maintaining vigorous stirring. After this step, the mixture was heated at 85 ± 3 °C for 30 min under stirring (7000 rpm). The co-precipitated magnetic nanoparticles were then thoroughly washed with distilled water. The material was dried and kept at room temperature (25 °C).

2.5. Fucan coating of the magnetite nanoparticles

The coating of magnetite nanoparticles with the polysaccharide fucan was achieved by the adsorption method. The fucan solution in distilled water (50 mg/mL) was added to the previously obtained magnetite nanoparticles (100 mg) and maintained at 25 °C for 16 h under stirring. Afterward, the coated nanoparticles were thoroughly washed with distilled water. The material was dried and kept at room temperature (25 °C).

2.6. Physical and chemical characterization of the magnetics nanoparticles

The obtained uncoated and the fucan-coated MNPs were characterized by different techniques. The surface morphology was observed through a field emission scanning electron microscope (SEM, FEI model Quanta-200F); the size of the MNPs as measured through transmission electron microscopy (TEM, TECNAI G2 Spirit—FEI Company) with an acceleration voltage of 80 kV. The SEM samples were prepared by dropping a dilute suspension of powder on a glass and the surface was coated with a thin gold film under vacuum prior to microscopy scanning. For TEM analysis, the samples were deposited on copper grids of 400 mesh coated with carbon. The crystalline properties and phase identification were characterized by X-ray diffraction (XRD), using a Siemens D5000 diffractometer. The diffratogram was obtained by using Cu-Kα radiation ($\lambda = 1.5406$ Å) in the range $10^\circ < 2\theta^\circ < 80^\circ$ with steps of 0.02° and acquisition time of 1.0 s/step. The surface functionalization was characterized by a Bruker IFS-66 Fourier transform infrared (FT-IR) spectroscope. These measurements were performed in the frequency interval of 4000–400 cm^{-1} with resolution of 1.29 cm^{-1}. A conventional transmission Mossbauer spectrometer was employed at room temperature (RT) using 1024 channels. The source was cobalt-57 in a rhodium matrix moving with sinusoidal mode at RT. Isomer shifts were given with respect to metallic iron at RT. The magnetic properties of the MNPs were measured on an MPMS−5S (Magnetic Property Measurement System) magnetometer from Quantum Design, with a sensor SQUID (Superconducting Quantum Interference Device). The measurements were taken at room temperature (25 °C) and under different applied magnetic fields from −7 to +7 kOe.

3. Results and discussion

The surface morphology and size of the neat MNPs and the fucan-coated MNPs were observed by SEM and TEM (see Fig. 1). In Fig. 1(a), the uncoated nanoparticles are shown. As expected, aggregate of particles occurred since the specific surface area (surface-to-volume ratio) is large resulting in a high surface energy. This is better appreciated in Fig. 1(c), in which one group of uncoated nanoparticles is shown. From the image, we can find that most of the uncoated nanoparticles are quasi-spherical with a mean size around 10 nm. After fucan coating, the aggregation was reduced and the nanoparticle dispersion was improved (see Fig. 1(b) and (d)). The lack of

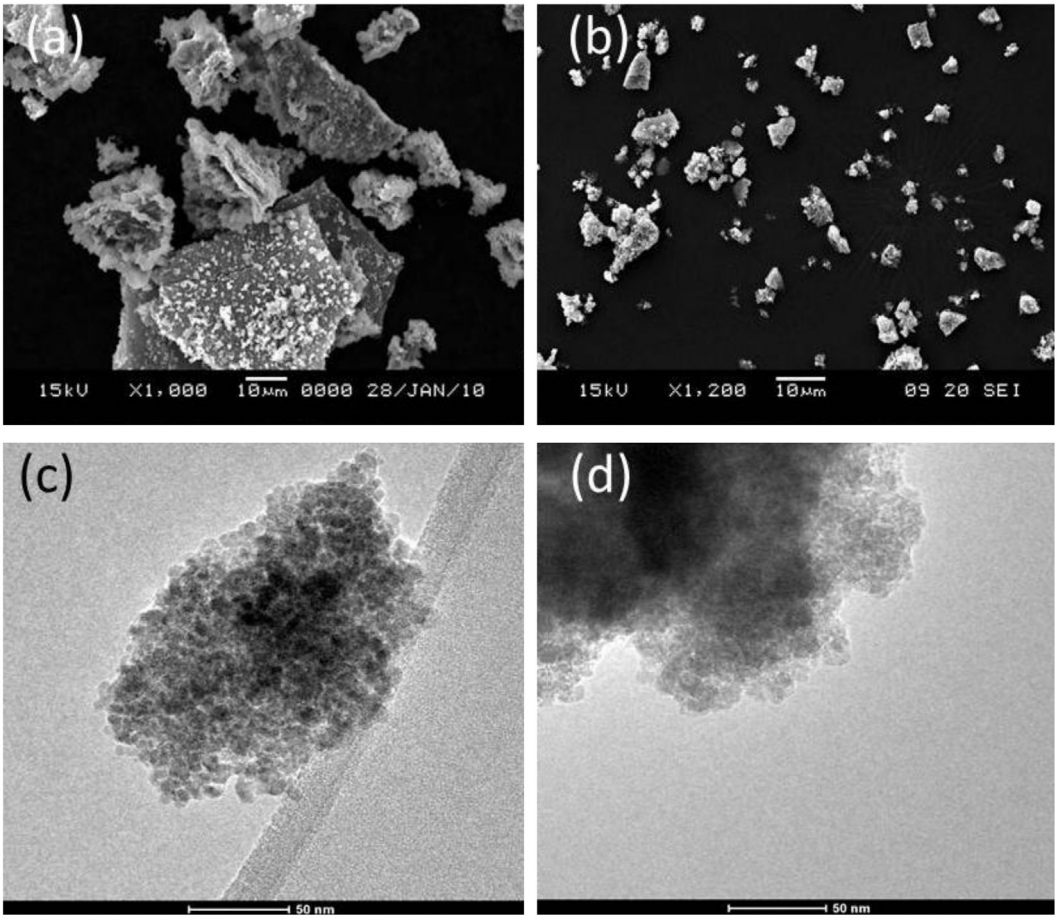

Fig. 1. SEM and TEM micrographs of uncoated and fucan-coated MNPs. (a) SEM of the uncoated MNPs; (b) SEM of fucan-coated MNPs; (c) TEM of the uncoated MNPs and (d) TEM of fucan- coated MNPs.

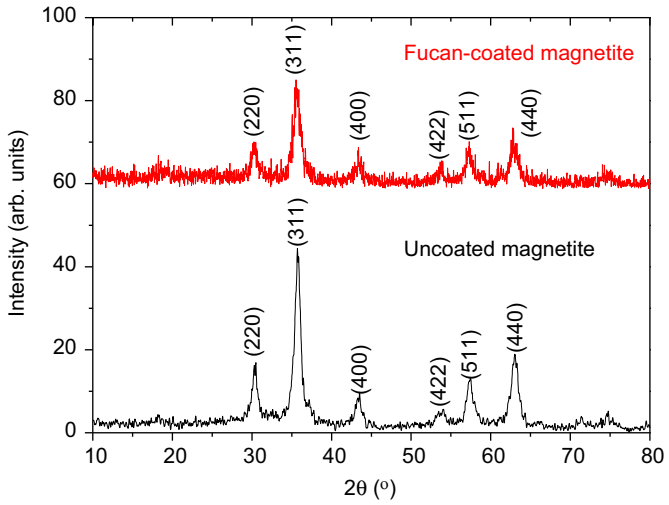

Fig. 2. XRD patterns of the fucan-coated (top) and the uncoated (bottom) magnetite MNPs.

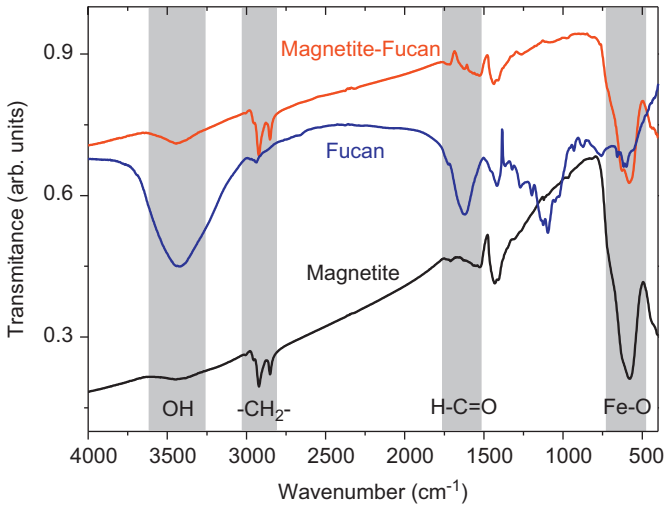

Fig. 3. FT-IR spectra from the fucan polyssacharide and from the uncoated and fucan-coated magnetite nanoparticles.

aggregation is probably because the fucan coating weakens the magnetic interactions between particles.

Fig. 2 shows the X-ray powder diffractograms of the uncoated and fucan-coated MNPs. From the patterns, a series of characteristic peaks (2 2 0), (3 1 1), (4 0 0), (4 2 2), (5 1 1), and (4 4 0), which are in well accordance with the inverse cubic spinel phase of Fe_3O_4 (magnetite, JCPDS card no. 85-1436), were observed. These results are similar to those reported in the literature [37]. The mean crystallite diameter obtained from the diffractogram by using the Scherrer's formula [38] is 10 nm, which confirms the size observed by the electron micrographs above. The fucan-coated MNPs diffractogram shows the same peaks as those of uncoated MNPs, indicating that the functionalization does not degrade the core magnetite. However, it is notable that in the case of the fucan-coated magnetite, the peaks height decreased and the background became noisy. This correctly indicates that the peak reflections are originated from the

core magnetite and the noisy background comes from the amorphous dried polysaccharide shells. Similar results were obtained by Hong et al. (2008) [39] for dextran-coated magnetite MNPs.

FT-IR spectroscopy was used to study the functionalization of the magnetite nanoparticles with fucan. Fig. 3 illustrates the FT-IR spectra from fucan, magnetite and fucan-coated magnetite. From all the spectra, except for that of fucan, it is possible to see a deep peak at about 571 cm^{-1} characteristics of the Fe–O bond absorption. This confirms the presence of the magnetic core and thus it is more pronounced in the bare magnetite nanoparticles. The absorption peak at about 3400 cm^{-1} is observed in all specta and it is the widest in the fucan spectrum. This may be originated by hydroxyls (OH) present in water and polysaccharides. By comparing the spectra of the coated and the uncoated magnetites, it is observed that the band around 3400 cm^{-1} is more pronounced and broader in the coated nanoparticles than in the bare nanoparticles, indicating the presence of the polysaccharide shell. The band at about 1619 cm^{-1} in the fucan spectra represents the stretching vibration of its H–C═O backbone. Note that this band is much more intense in fucan alone than in the coated magnetite and the uncoated magnetite, and it is more intense in fucan-coated magnetite than in uncoated magnetite, as expected. The band around 1095 cm^{-1} in the fucan spectra is characteristic of hemiacetal vibration which is present in ether and alcohol groups from fucose. The bands around 2921 cm^{-1} and 2851 cm^{-1} are assigned to stretching vibration of $-CH_2$ groups, indicating the presence of oleic acid. Therefore, the FT-IR confirms the functionalization of the Fe_3O_4 nanoparticles with the fucan polissacharides.

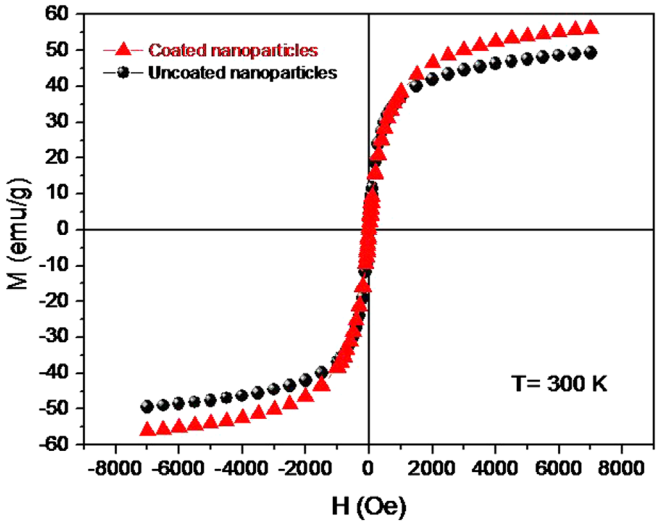

Fig. 4. Magnetization curves of the Fe_3O_4 nanoparticles: uncoated (circle) and fucan coated (triangle).

The measurements of the magnetic field-dependence of the magnetization of the uncoated and coated magnetite nanoparticles at 300 K are presented in Fig. 4. The plots indicate that both samples exhibit superparamagnetic behavior with zero remanence and coercivity. The superparamagnetic behavior is mainly generated by the magnetite cores in each sample. The saturation magnetization (M_S), determined by using the law of approach to saturation, is around 50 emu/g for the uncoated Fe_3O_4 NPS. This saturation magnetization value is consistent with the value reported in the literature for magnetite NPS with sizes around 10 nm [40]. However, it is observed that in the case of the coated magnetite, the magnitude of magnetization is higher than in the bare MNPs. This effect should be caused by magnetic disorder existing on the surface of magnetite MNPs due to the effect of external media interactions (i.e interaction between particles). In this sense, fucan coating weakens the interaction between

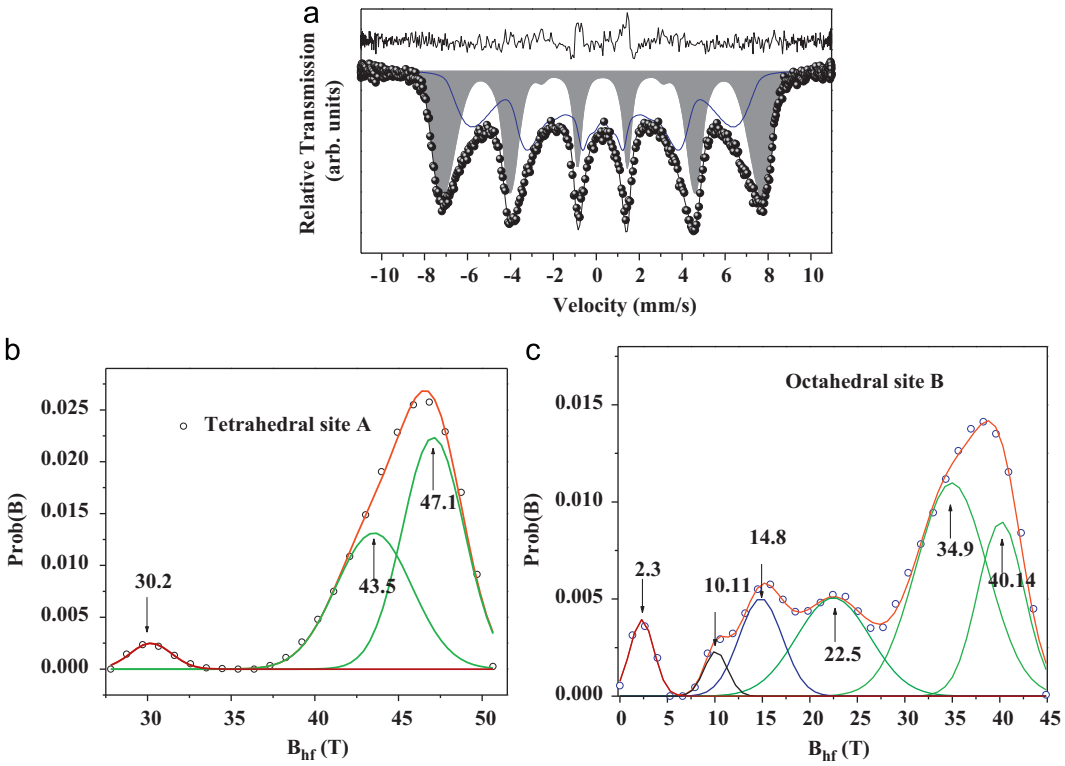

Fig. 5. (a) RT Mössbauer spectra of the uncoated nanomagnetite sample showing tetrahedral site A (large gray shadow) and octahedral site B (fine blue line). The points represent the experimental data and the residual is shown in the top part. Hyperfine distribution deconvoluted for tetrahedral site A. (b) and octahedral site B (c). (For interpretation of the references to color in this figure legend, the reader is referred to the web version of this article.)

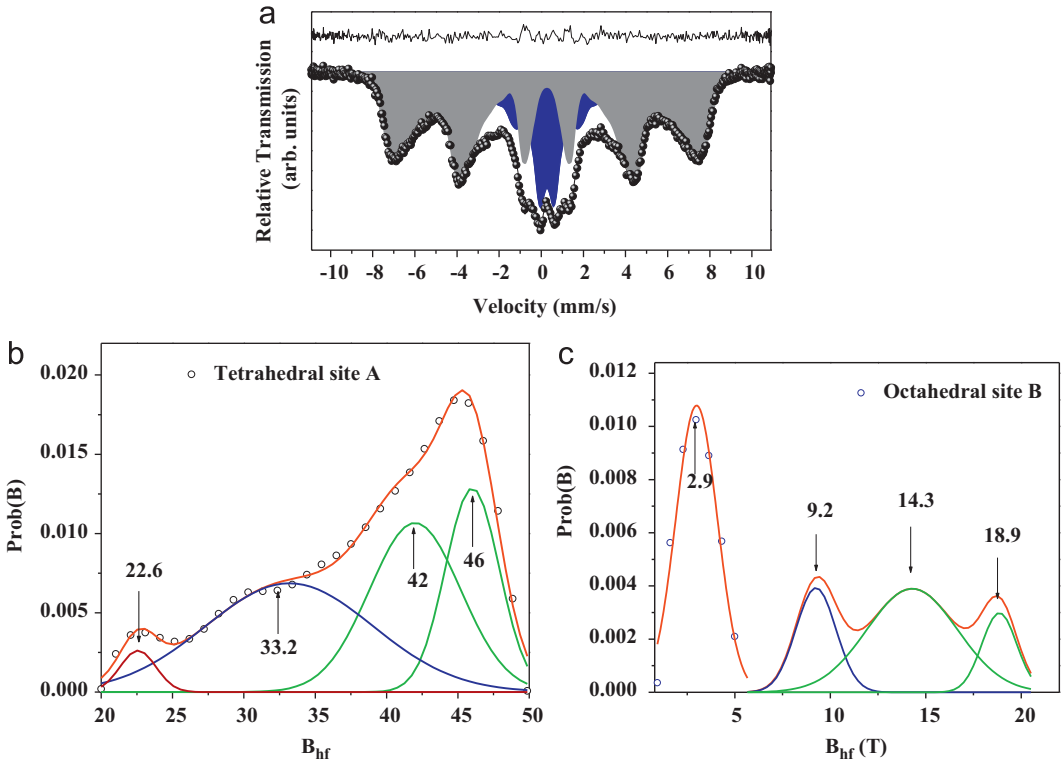

Fig. 6. RT Mössbauer spectra of the nanomagnetite coated with fucan showing tetrahedral site A (large gray shadow) and octahedral site B (center blue shadow). The points represent the experimental data and the residual is in the top part. Deconvoluted hyperfine distribution for tetrahedral site A (b) and octahedral side B (c). (For interpretation of the references to color in this figure legend, the reader is referred to the web version of this article.)

particles, which in turns reduces the disorder of the spins on the surface, thus increasing the magnetization. Similar effects have been reported for surface-passivated magnetic nanoparticles which have been assigned to the improvement of crystalline quality [41]. Moreover, those saturation magnetization values are significantly lower than the value reported for bulk Fe_3O_4 (M_S~82 emu/g). These lower saturations must be related to the surface effects such as oxidation [42–44]. These effects must be the responsible for the increasing tendency of the M vs. H curve observed in the high-field region.

Fig. 5 shows the Mössbauer spectra and its corresponding hyperfine magnetic field distribution of the uncoated Fe_3O_4 nanoparticles at RT. Fig. 5(a) shows a sextet of widened lines fitted with two hyperfine field distributions. The first corresponds to the magnetic Fe^{3+} in tetrahedral site A and the second represents the octahedral site B of magnetite [45]. The hyperfine magnetic field distribution for site A (Fig. 5(b)) shows three peaks 47.1, 43.5 and 30.2 T, which were calculated through three Gaussian functions. For the distribution of site B (Fig. 5(c)), six Gaussian functions centered at 40.14, 34.9, 22.5, 14.8, 10.11 and 2.3 T, were necessary. This is typical of superparamagnetic relaxation due to the presence of small particles (~10 nm). In this case, the magnetic moment of each individual particle fluctuates along an easiest axis of magnetization.

Fig. 6 shows the Mössbauer spectra at RT of the magnetite nanoparticles coated with fucan and its corresponding hyperfine magnetic field distribution. Similar to the case of the magnetite, the spectrum was fitted using two distributions. The first is associated to a tetrahedral site A containing a sextet with broadened linewidth. For site B, the relaxation is observed for the octahedral site due a reduced magnetic dipole–dipole interaction produced by the fucan coating, which was observed in magnetization measurements (Fig. 3) and also in other systems [46]. The hyperfine magnetic field distribution for site A (Fig. 6(b)) shows four peaks, whose centers were calculated through four Gaussian functions: 46.0, 42.0, 33.2 and 22.6 T, for a range of magnetic fields between 20.0 and 49.87 T covering an area of 70.80%. For the distribution of site B, four Gaussian peaks whose centers are at 18.9, 14.3, 9.2 and 2.9 T were necessary for a range of magnetic fields between 0.94 and 20.51 T with an area of 29.20%.

4. Conclusions

In summary, we obtained fucan-coated magnetite nanoparticles by co-precipitation syntheses method. XRD diffractograms and FT-IR absorption spectra confirmed that the magnetite nanoparticles were obtained and they were successfully coated. TEM micrographs revealed that both the uncoated and fucan-coated magnetite nanoparticles have sizes around 10 nm. Magnetic measurements and Mössbauer spectroscopy at RT revealed that the superparamagnetic property of the Fe_3O_4 nanoparticles is affected by the fucan polysaccharide coating, thus preventing aggregation.

Acknowledgments

This work was supported by the Brazilian science agencies Coordenação de Aperfeiçoamento de Pessoal de Nível Superior (CAPES), the Conselho Nacional de Desenvolvimento Científico e Tecnológico (CNPq) and the Fundação de Amparo à Ciência e Tecnologia do Estado de Pernambuco (FACEPE) (APQ-0589-1.05/08).

References

[1] V.I. Shubayev, T.R. Pisanic, S. Jin, Magnetic nanoparticles for theragnostics, Advanced Drug Delivery Reviews 61 (2009) 467–477.
[2] W.H. Suh, K.S. Suslick, G.D. Stucky, Y. Suh, Nanotechnology, nanotoxicology, and neuroscience, Progress in Neurobiology 87 (2009) 133–170.

[3] L. De Los Santos Valladares, J. Llandro, D.W. Lee, T. Mirelias, J.J. Palfreyman, T.J. Hayward, J. Cooper, J.A.C. Bland, C.H.W. Barnes, J.L. Arroyo, M. Lees, Journal of Magnetism and Magnetic Materials 321 (2009) 2129–2134.
[4] L. Cabrera, S. Gutierrz, N. Menendez, M.P. Morales, P. Herrasti, Magnetite nanoparticles: electrochemical synthesis and characterization, Electrochimica Acta 53 (2008) 3436–3441.
[5] T.K. Jain, J. Richey, M. Strand, D.L. Leslie-Pelecky, C.A. Flask, V. Labhasetwar, Magnetic nanoparticles with dual functional properties: drug delivery and magnetic resonance imaging, Biomaterials 29 (2008) 4012–4021.
[6] A. Kumar, K.J. Prasanna, S. Behera, R.F. Lockey, S.M. Monapatra, A.M. Shy, Multifunctional magnetic nanoparticles for targeted delivery, Nanomedicine 6 (2010) 64–69.
[7] Y. Zhan, F. Meng, X. Yang, R. Zhao, X. Liu, Solvothermal synthesis and characterization of functionalized graphene sheets (FGSs)/magnetite hybrids, Materials Science and Engineering B 176 (2011) 333–1339.
[8] J. Corchero, A. Villaverde, Biomedical applications of distally controlled magnetic nanoparticles, Trends in Biotechnology 27 (2009) 468–476.
[9] M. Rahimi, A. Wadajkar, K. Subramanian, M. Yousef, W. Cui, J. Hsieh, K. Nguyen, In vitro evaluation of novel polymer-coated magnetic nanoparticles Q13 for controlled drug delivery, Nanomedicine 6 (2010) 672–680.
[10] L.Y. Zhang, X.J. Zhu, H.W. Sun, G.R. Chi, J.X. Xu, Y.L. Sun, Control synthesis of magnetic Fe_3O_4–chitosan nanoparticles under UV irradiation in aqueous system, Current Applied Physics 10 (2010) 828–833.
[11] A. Bandhu, S. Mukherjee, S. Acharya, S. Modak, S.K. Brahma, D. Das, P.K. Chakrabarti, Dynamic magnetic behaviour and Mössbauer effect measurements of magnetite nanoparticles prepared by a new technique in the co-precipitation method, Solid State Communications 149 (2009) 1790–1794.
[12] G.J.A. Ramos, A. Bustamante, J. Flores, S.M. Mejía, A..Osorio Anaya, A.I. Martínez, L. De Los Santos Valladares, C.H.W. Barnes, Hyperfine Interactions 2013, special volume LACAME 2012.
[13] J. Ding, K. Tao, J. Li, S. Song, K. Sun, Cell-specific cytotoxicity of dextran-stabilized magnetite nanoparticles, Colloids and Surfaces B: Biointerfaces 79 (2010) 184–190.
[14] P.L. Andrade, V.A.J. Silva, J.C. Maciel, M.M. Santillan, N.O. Moreno, L. De Los Santos Valladares, A. Bustamante, S.M.B. Pereira, M.P.C. SilvaJ. Albino Aguiar, Hyperfine Interactions 2013, special volume LACAME 2012.
[15] L. León-Félix, J. Chaker, M. Parise, J.A.H. Coaquira, L. De Los Santos Valladares, A. Bustamante, V.K. Garg, A.C. Oliveira, P.C. Morais, Hyperfine Interactions 2013, special volume LACAME 2012.
[16] S.B. Darling, S.D. Bader, Journal of Materials Chemistry B 15 (2005) 4189–4195.
[17] J. Chomoucka, J. Drbohlavova, D. Huska, V. Adam, R. Kizek, J. Hubalek, Magnetic nanoparticles and targeted drug delivering, Pharmacological Research 62 (2010) 144–149.
[18] Z.L. Liu, H.B. Wang, Q.H. Lu, G.H. Du, L. Peng, Y.Q. Du, S.M. Zhang, K.L. Yao, Synthesis and characterization of ultrafine well-dispersed magnetic nanoparticles, Journal of Magnetism and Magnetic Materials 283 (2004) 258–262.
[19] P.M. Araujo, G.B. Oliveira, C.R. Cordula, E.L. Leite, L.B. Carvalho, M.P.C. Silva, Sulfated fucan as support for antibiotic immobilization, Brazilian Journal of Medical and Biological Research 37 (2004) 301–305.
[20] S.J. Yoon, Y.R. Pyun, J.K.H. Wang, P.A.S. Moura, A sulfated fucan from the brown alga *Laminaria cichorioides* has mainly heparin cofactor II dependent anticoagulant activity, Carbohydrate Research 342 (2007) 2326–2330.
[21] K.C.S. Queiroz, V.P. Medeiros, L.S. Queiroz, L.R.D. Abreu, H.A.O. Rocha, C.V. Ferreira, M.B. Juca, H. Aoyama, E.L. Leite, Inhibition of reverse transcriptase activity of HIV by polysaccharides of brown algae, Biomedicine and Pharmacotherapy 62 (2008) 303–330.
[22] P. Karmakar, T. Ghosh, S. Sinha, S. Saha, P. Mandal, P.K. Ghosal, B. Ray, Polysaccharides from the brown seaweed *Padina tetrastromatica*: characterization of a sulfated fucan, Carbohydrate Polymers 78 (2009) 416–421.
[23] N.P. Chandıa, B. Matsuhiro, Characterization of a fucoidan from *Lessonia vadosa* (Phaeophyta) and its anticoagulant and elicitor properties, International Journal of Biological Macromolecules 42 (2008) 235–240.
[24] T.C.G. Azevedo, M.E.B. Bezerra, M.G.L. Santos, L.A. Souza, C.T. Marques, N.M.B. Benedives, E.L. Leite, Heparinoids algal and their anticoagulant, hemorrhagic activities and platelet aggregation, Biomedicine and Pharmacotherapy 63 (2009) 477–483.
[25] C.J. McCormick, C.I. Newbold, A.R. Berendt, Sulfated glycoconjugates enhance CD36-dependent adhesion of *Plasmodium falciparum*-infected erythrocytes to human microvascular endothelial cell, Blood 96 (2000) 327–333.
[26] A. Cumashi, N.A. Ushakova, M.E. Preobrazhenskaya, A. D'Incecco, A. Piccoli, L. Totani, A comparative study of the anti-inflammatory, anticoagulant, anti-angiogenic and anti-adhesive activities of nine different fucoidans from brown seaweeds, Glycobiology 17 (2007) 541–552.
[27] P.A.S. Mourão, Use of sulfated fucans as anticoagulant and antithrombica-gents: future perspective, Current Pharmaceutical Design 10 (2004) 967–981.
[28] B. Tissot, R. Daniel, Biological properties of sulfated fucans: the potent inhibiting activity of algal fucoidan against the human complement system, Glycobiology 13 (2003) 29G–31G.
[29] Y.L. Chew, Y.Y. Lim, M. Omar, K.S. Khoo, Antioxidant activity of three edible seaweeds from two areas in South East Asia, LWT—Food Science and Technology 41 (2008) 1067–1072.
[30] M.K. Patel, B. Mulloy, K.L. Gallagher, L. O'Brien, A.D. Hughes, The antimitogenic action of the sulfated polysaccharide sulfated fucan differs from heparin in human vascular smooth muscle cells, Thrombosis and Haemostasis 87 (2002) 149–154.
[31] T. Nishino, A. Fukuda, T. Nagumo, M. Fujihara, E. Kaji, Inhibition of the generation of thrombin and factor Xa by a sulfated fucan from the brown seaweed *Ecklonia kurome*, Thrombosis Research 96, 1999, 37–49.
[32] I.P. Alwayn, J.Z. Appel, C. Goepfert, L. Buhler., D.K. Cooper, S.C. Robson, Inhibition of platelet aggregation in baboons: therapeutic implications for xenotransplantation, Xenotransplantation 7 (2000) 247–257.
[33] T.V. Alekseyenko, S.Y. Zhanayeva, A.A. Venediktova, T.N. Zvyagintseva, T.A. Kuznetsova, N.N. Besednova, Antitumor and antimetastatic activity of fucoidan, a sulfated polysaccharide isolated from the Okhotsk sea Fucus evanescens brown alga, Bulletin of Experimental Biology and Medicine 147 (2007) 730–732.
[34] T. Ghosh, K. Chattopadhyay, M. Marschall, P. Karmakar, P. Mandal, B. Ray, Focus on antivirally active sulfated polysaccharides: from structure activity analysis to clinical evaluation, Glycobiology 19 (2009) 2–15.
[35] M. Dubois, K.A. Gilles, J.K. Hamilton, P.A. Rebers, F. Smith, Colorimetric method for determination of sugars and related substances, Analytical Chemistry 28 (1956) 350–356.
[36] A.M.A. Carneiro Leão, E.A. Oliveira, L.B. Carvalho Jr., Immobilization of protein on ferromagnetic dacron, Biotechnology and Applied Biochemistry 32 (1991) 53–58.
[37] Y.M. Wang, X. Cao, G.H. Liu, R.Y. Hong, Y.M. Chen, X.F. Chen, H.Z. Li, B. Xu, D.G. Wei, Synthesis of Fe_3O_4 magnetic fluid used for magnetic resonance imaging and hyperthermia, Journal of Magnetism and Magnetic Materials 323 (2011) 2953–2959.
[38] B. Dennnis, Cullity, Elements of X-ray Diffraction, third ed., Prentice-Hall International, Upper Saddle River, NJ, London, 2000.
[39] R.Y. Hong, B. Feng, L.L. Chen, G.H. Liu, H.Z. Li, Y. Zheng, D.G. Wei, Synthesis, characterization and MRI application of dextran-coated Fe_3O_4 magnetic nanoparticles, Biochemical Engineering Journal 42 (2008) 290–300.
[40] G.F. Goya, T.S. Berquó, F.C. Fonseca, M.P. Morales, Journal of Applied Physics 94 (2003
) 3520–3528.
[41] M.I. Oshtrakh, M.V. Ushakov, A.S. Semenova, D.G. Kellerman, V. Sepelák, A.F.R. Rodriguez, V.A. Semionkin, P.C. Morais, Hyperfine Interactions 219, 2013, 19–24.
[42] S.H. Gee, Y.K. Hong, D.W. Erickson, M.H. Park, J.C. Sur, Journal of Applied Physics 93 (2003) 7560.
[43] M.P. Morales, S. Veintemillas Verdager, M.I. Montero, C.J. Serna, A. Roig, L.I. Casas, B. Martinez, F. Sandiumengue, Chemistry of Materials 11 (1999) 3058.
[44] J. Korecki, B. Handke, N. Spiridis, T. Slezak, I. Flis-Kabulska, J. Haber, Thin Solid Films 412 (2002) 14.
[45] R.V. Ferreira, I.L.S. Pereira, L.C.D. Cavalcante, L.F. Gamarra, S.M. Carneiro, E. Amaro Jr., J.D. Fabris, R.Z. Dominguez, A.L. Andrade, Hyperfine Interactions 195 (2010) 265–274.
[46] R. Ghosh, L. Pradhan, Y. Priyabala Devi, S.S. Meena, R. Tewari, Amit Kumar, S. Sharma, N.S. Gajbhiye, R.K. Vatsa, B.N. Pandey, R.S. Ningthoujam, Journal of Materials Chemistry 21 (2011) 13388.